

# Steady free-surface flow over spatially periodic topography

B. J. Binder<sup>1†</sup>, M. G. Blyth<sup>2</sup>  
and S. Balasuriya<sup>1</sup>

<sup>1</sup>School of Mathematical Sciences, University of Adelaide, South Australia, Australia

<sup>2</sup>School of Mathematics, University of East Anglia, Norwich, UK.

(Received 25 August 2015)

Two-dimensional free-surface flow over a spatially periodic channel bed topography is examined using a steady periodically-forced Korteweg-de Vries equation. The existence of new forced solitary-type waves with periodic tails is demonstrated using recently developed non-autonomous dynamical systems theory. Bound-states with two or more co-existing solitary waves are also identified. The solution space for varying amplitude of forcing is explored using a numerical method. A rich bifurcation structure is uncovered and shown to be consistent with an asymptotic theory based on small forcing amplitude.

## 1. Introduction

The interaction between bottom topography and surface waves in open channel flow is an important topic motivated in part by environmental considerations such as the impact on erodible beds in streams or rivers (e.g. Reynolds 1965; Davies & Heathershaw 1984). A substantial literature is devoted to the generation of surface waves in flow over topography (see, for example, Lamb 1879; Lighthill 1978; Shen 1993; Wu 1987). In the present work we examine the problem of steady two-dimensional flow past an infinitely long impermeable spatially periodic channel bed. To model the stationary surface wave pattern which is generated by a periodic bottom topography, we use the steady form of the well-known forced Korteweg De Vries (fKdV) equation, which describes the free-surface elevation in response to a prescribed forcing.

In the present context, the fKdV equation is valid when the deflection of the free surface from a flat state and the amplitude of the bottom topography are both small, and when the Froude number for the flow is close to unity. The equation also applies in other flow problems, notably the resonant sloshing of water in a horizontally oscillating tank (e.g. Ockendon & Ockendon 1973; Cox & Mortell 1986; Ockendon *et al.* 1986; Amundsen *et al.* 2007). Its popularity stems from its relative simplicity and utility—as a single equation flow model—and from the fact that it provides insight into the effects of weak nonlinearity and dispersion without solving the corresponding fully nonlinear problem. In the present case, it permits a detailed parametric study of a rich and diverse solution space revealing the existence of new solitary-type wave solutions for flow over an uneven bed.

The dimensionless form of the steady fKdV equation is given by (Akylas 1984; Binder *et al.* 2005; Cole 1985; Dias & Vanden-Broeck 2002; Grimshaw & Smyth 1986; Shen 1993)

$$\eta_{xx} + \frac{9}{2}\eta^2 - 6\mu\eta = -3\sigma(x), \quad (1.1)$$

† Email address for correspondence: benjamin.binder@adelaide.edu.au

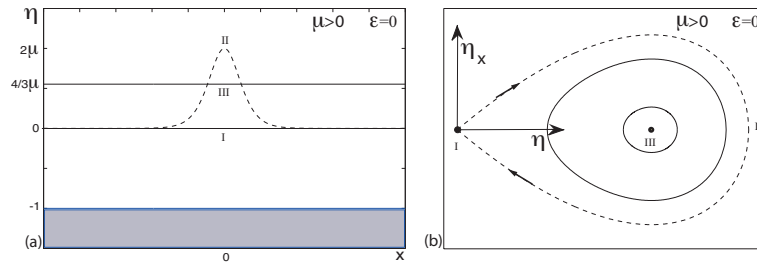


FIGURE 1. Sketches of the three unforced solutions,  $\epsilon = 0$ ,  $\mu > 0$ . (a) Physical plane,  $(x, \eta)$ . The upper solid line is the uniform cnoidal stream solution III,  $\eta(x) = 4\mu/3$ . The lower solid line is the uniform stream solution I,  $\eta(x) = 0$ . The broken curve is the solitary wave solution II,  $\eta(0) = 2\mu$ . The shaded region,  $\eta(x) \leq -1$ , is the flat channel bed. (b) Autonomous phase plane,  $(\eta, \eta_x)$ . The saddle point located at the origin is solution I. The centre located at  $(4\mu/3, 0)$  is solution III. The homoclinic orbit is solution II.

where  $\eta(x)$  is the free-surface elevation relative to a uniform stream,  $\sigma(x)$  is a prescribed forcing representing the channel bottom topography, and  $\mu$  is a real parameter related to the Froude number. Some background detail on the form of (1.1) is given in Other Supplementary Material (OSM) Appendix A.

In the majority of this present work, we adopt the sinusoidal forcing,

$$\sigma(x) = \epsilon \cos kx, \quad (1.2)$$

where  $\epsilon$  and  $k$  are the amplitude and wavenumber of the forcing, respectively, both of which are arbitrary. The problem is governed by the dimensionless parameters  $k$ ,  $\epsilon$  and  $\mu$ .

With  $\epsilon = 0$ , Binder et al. (2005) and others have shown that equation (1.1) can be expressed as a two-dimensional non-linear dynamical system with two fixed points. The classification of the fixed points depends on whether  $\mu < 0$  or  $\mu > 0$ . If we initially restrict attention to the case when  $\mu > 0$ , the first of these points lies at the origin of the  $(\eta, \eta_x)$  phase plane and corresponds to a saddle point, as is illustrated in figure 1b. It represents a uniform stream (herein termed solution I) with  $\eta(x) = 0$ . The homoclinic orbit connecting the fixed point at the origin to itself, seen as a broken line in figure 1b, corresponds to the classical unforced solitary wave (solution II) given by

$$\eta(x) = 2\mu \operatorname{sech}^2 \left( \sqrt{\frac{3\mu}{2}} x \right). \quad (1.3)$$

Both solution types I and II satisfy the far-field uniform flow condition ( $\eta_{xx} \rightarrow 0$ ,  $\eta_x \rightarrow 0$ ,  $\eta \rightarrow 0$  as  $x \rightarrow \pm\infty$ ) used in the derivation of equation (1.1). The second fixed point is located at  $(\eta, \eta_x) = (4\mu/3, 0)$  in the phase plane and corresponds to a centre. The closed trajectories centred around this fixed point are usually called cnoidal waves, and can be expressed in closed form using Jacobi elliptic functions (Billingham & King 2000). The second fixed point at  $\eta = 4\mu/3$  represents another constant-level solution, which we term a uniform *cnoidal* stream (solution III). This solution appears to lack physical relevance as it violates the far-field flow condition  $\eta \rightarrow 0$  used in the derivation of equation (1.1). However, we note that if we perform the replacement

$$\eta \rightarrow \eta + 4\mu/3, \quad \text{followed by} \quad \mu \rightarrow -\mu \quad (1.4)$$

to (1.1), we recover the same equation. This invariance means that this second fixed

point is associated with a solution satisfying  $\eta, \eta_x, \eta_{xx} \rightarrow 0$  in the far-field for a *different*  $\mu$  value, and hence has physical relevance.

To retain consistency, we shall initially characterise all the possible subtypes of perturbed solutions for the same value of  $\mu > 0$ . The unforced solutions I–III are shown in the physical plane in figure 1a. When  $\sigma(x) \neq 0$ , these three types of solutions—near-uniform, solitary and cnoidal—perturb. The focus of this article is to characterise exactly these forced solutions, for which we obtain explicit analytical wave profiles. We remark that our equations (1.1) and (1.2) are similar to those considered by Grimshaw & Tian (1994) who demonstrated that the system possessed chaotic solutions. The forced solitary-type wave (type II) is the specific type of solution which leads to the presence of nearby chaotic solutions, in the sense that it corresponds exactly to the intersection of stable and unstable manifolds which is necessary to establish that the system is chaotic (Guckenheimer & Holmes 1983).

We compute numerical solutions of (1.1) using the scheme described in OSM Appendix B. Typical elevation profiles for  $\mu = 0.1$ ,  $k = 3.0$  and  $|\epsilon| = 0.1$  are presented in figure 2. Figure 3 shows the bifurcation structure for the case  $\mu = 0.1$ , in which the numerics show excellent correspondence with the analytical approximations for types I and II (derived in section 2), and type III (derived in section 3). In section 4, we further analyse the morphology of the solutions when  $\mu > 0$ , and consider two other types of forcing in a flow regime when  $\mu < 0$ .

## 2. Type I and II solutions: non-autonomous theory

The uniform stream and solitary wave solutions of the autonomous system (1.1) with no forcing are represented respectively by the fixed point at the origin and its homoclinic connection in figure 1b. ‘Homoclinic’ means that a branch of the stable and unstable manifold of the fixed point coincide, and hence the associated wave approaches  $(\eta, \eta_x) = (0, 0)$  as  $x \rightarrow \pm\infty$ . Inclusion of the forcing term (i.e.,  $\epsilon \neq 0$ ) renders the system non-autonomous. To understand this, we adapt the recently developed theory of Balasuriya & Binder (2014), a detailed discussion of which is provided in OSM Appendix C. For  $|\epsilon| \ll 1$ , it can be shown that there is only one solution which remains  $\mathcal{O}(\epsilon)$ -close to the uniform stream (i.e., the saddle fixed point in figure 1b) over the entire unbounded domain, and this is given by

$$\eta^I(x) = \frac{3\epsilon \cos(kx)}{k^2 + 6\mu} \quad (2.1)$$

to  $\mathcal{O}(\epsilon^2)$ . The dotted curves in figure 2a are for this near-uniform solution (2.1), which is the non-autonomous type-I solution.

Next, we consider solutions which are near-solitary. These are solutions which have one big hump with height approximately  $2\mu$ , overlaid with smaller oscillations, and which decay in the far field to the near-uniform solution (2.1). This is the only natural far-field possibility for near-solitary waves in this non-autonomous setting, since the only solution which remains approximately uniform as  $x \rightarrow \pm\infty$  is (2.1). The dynamical-systems interpretation is that these are homoclinic trajectories to (2.1) which are near to a corresponding homoclinic trajectory to the autonomous system. When  $\epsilon = 0$ , there were an uncountable number of one-humped solitary waves obtained by taking arbitrary shifts of (1.3). When  $|\epsilon| \ll 1$  but is nonzero, the non-autonomous theory of Balasuriya & Binder (2014) can be adapted to characterise all one-humped solitary waves. As derived in OSB Appendix C, there are exactly two possible types of such one-humped solitary waves: (i) those centred around crests, and (ii) those centred around troughs of

the topography. Near-solitary waves within each of these two families are simple shifts of each other by multiples of  $k\pi$ . For example, if  $\epsilon > 0$ , there is a crest of  $\sigma$  at  $x = 0$ , resulting in a crest-centred near-solitary wave centred at  $x = 0$ . Other crest-centred near-solitary waves can be obtained by shifting this to the values  $x = 2n\pi/k$ ,  $n \in \mathbb{Z}$ . Trough-centred near-solitary waves would therefore be centred at  $x = (2n + 1)\pi/k$ ,  $n \in \mathbb{Z}$ . In contrast to the autonomous situation, there are only a *countable* number of such one-humped near-solitary waves. As described in OSM Appendix C, these near-solitary waves are the only ‘regular’ structures among ‘nearby’ solutions which are well-known to be chaotic (Grimshaw & Tian 1994), exhibiting seemingly random  $\mathcal{O}(1)$  excursions.

The one-humped non-autonomous near-solitary waves can be expressed to  $\mathcal{O}(\epsilon)$  explicitly by adapting the theory of Balasuriya & Binder (2014), as described in detail in OSM Appendix C. The near-solitary wave centred at  $x = 0$  is given by

$$\eta^{II}(x) = \bar{\eta}(x) + \epsilon [\eta^n(x) + \eta^t(x)] + \mathcal{O}(\epsilon^2) \quad (2.2)$$

in which  $\bar{\eta}$  is the fundamental solitary wave solution (1.3),

$$\eta^n(x) = -\frac{3\bar{\eta}_{xx}(x)}{\bar{\eta}_x(x)^2 + \bar{\eta}_{xx}(x)^2} \int_{|x|}^{\infty} \bar{\eta}_x(\tau) \cos(k\tau) \, d\tau, \quad (2.3)$$

and

$$\eta^t(x) = -3\bar{\eta}_x(|x|) \int_0^{|x|} \frac{\bar{\eta}_{xx}(\tau) \cos(k\tau) - \Omega(\tau) \int_{|x|}^{\infty} \bar{\eta}_x(\lambda) \cos[k(\lambda + \tau - x)] \, d\lambda}{\bar{\eta}_x(\tau)^2 + \bar{\eta}_{xx}(\tau)^2} \, d\tau, \quad (2.4)$$

where

$$\Omega(\tau) := \frac{[6(1 + \mu) - 9\bar{\eta}(\tau) - 5] [\bar{\eta}_x(\tau)^2 - \bar{\eta}_{xx}(\tau)^2]}{\bar{\eta}_x(\tau)^2 + \bar{\eta}_{xx}(\tau)^2}. \quad (2.5)$$

The solution (2.2) is crest-centred if  $\epsilon > 0$ , and trough-centred if  $\epsilon < 0$ . Waves centred at other  $x$ -values can be computed from these solutions by simply shifting the wave solutions. The theoretical waves computed from (2.2) are virtually identical to the numerically computed solutions shown by the solid curves in figures 2b and 2d. To demonstrate this visually for curves which virtually fall on top of each other, we show the theoretical solution values computed from (2.2) on a coarse grid, shown by dots in figures 2b and 2d. The crest-centred solutions have an upwelling at the central crest, whereas the trough-centred ones have dips, as shown respectively in figures 2b and 2d.

The single-humped solitary waves are, as is clear from (2.2), symmetric about their central value. The presence of different single-humped solitary waves means that many-humped ones will exist as approximately the sum of several of the single-humped ones: figure 2e is composed from two trough-centred ones, while figure 2f has two trough-centred and one crest-centred one. Indeed, these figures were numerically obtained by using such a sum as an initial guess. Therefore, it is possible to form *multi-humped* solitary waves which are not symmetric.

While the above expressions are messy, the height at the central crest/trough at  $x = 0$  can be derived to be (see OSM Appendix C)

$$\eta^{II}(0) = 2\mu + \frac{\epsilon}{\mu} \left( k \int_0^{\infty} \operatorname{sech}^2 \left( \sqrt{\frac{3\mu}{2}} t \right) \sin(kt) \, dt - 1 \right). \quad (2.6)$$

The lower and upper broken straight lines in the panels of figure 3 correspond to values given by equations (2.1) and (2.6) respectively, demonstrating that the near-uniform and near-solitary waves obtained from the non-autonomous theory show excellent agreement with the numerics.

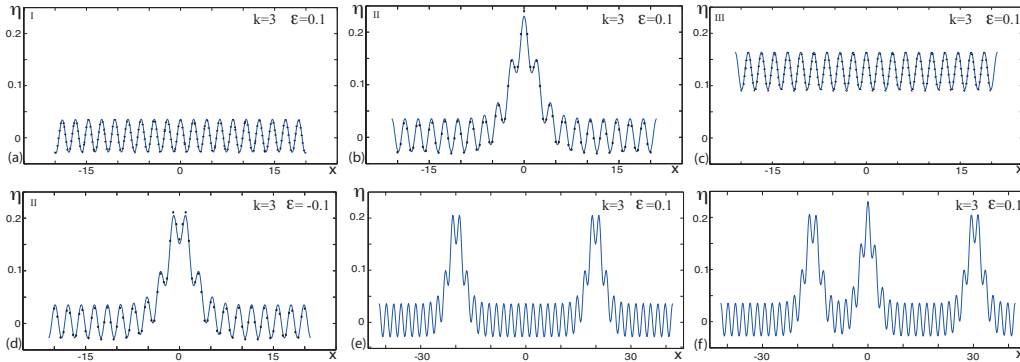


FIGURE 2. Free-surface profiles,  $\mu = 0.10$ ,  $k = 3.0$ ,  $|\epsilon| = 0.1$ . The solid curves are numerical solutions. The dotted curve in (a) is for the non-autonomous approximation, equation (2.1). The dotted curves in (b) and (d) are for the non-autonomous approximation, equation (2.2). The dotted curve in (c) is for the asymptotic theory, retaining only the first term in the regular expansion (3.2). (a) Perturbation of a uniform stream solution I,  $\eta(0) = 0.036$ ,  $\epsilon = 0.1$ . (b) Perturbation of a solitary wave solution II,  $\eta(0) = 0.231$ ,  $\epsilon = 0.1$ . (c) Perturbation of a uniform cnoidal stream solution III,  $\eta(0) = 0.167$ ,  $\epsilon = 0.1$ . (d) Perturbation of a solitary wave solution II,  $\eta(0) = 0.151$ ,  $\epsilon = -0.1$ . (e) and (f) Additional solutions,  $\epsilon = 0.1$ .

The near-solitary waves derived in this section are obtained explicitly in the unbounded  $x$ -domain for small topography, with no additional assumptions, matching conditions, or enforced spatial periodicity. Following a genuinely non-autonomous viewpoint helped to avoid such assumptions, which are often used in similar fKdV equations (e.g. Ockendon *et al.* 1986; Amundsen *et al.* 2007).

### 3. Type III solutions: asymptotic theory

As noted above, there exist unforced periodic cnoidal wave solutions to (1.1) when  $\epsilon = 0$ . To discuss the forced counterparts of such type III solutions we recast in terms of the shifted variable  $N(x) = \eta(x) - 4\mu/3$ , in which case (1.1), becomes

$$N_{xx} + \frac{9}{2}N^2 + \nu_c^2 N = -3\epsilon \cos kx, \quad (3.1)$$

where  $\nu_c = \sqrt{6\mu}$  is the frequency of small amplitude, unforced cnoidal waves which arise when  $\epsilon = 0$  and  $N \ll 1$ . It is now clear from (3.1) that resonance may occur for small amplitude waves if  $k = \nu_c$ . Furthermore, nonlinear generation of higher harmonics via the second term on the left hand side of (3.1) raises the prospect of secondary resonances at  $k = \nu_c/2^n$  for  $n = 2, 3, 4, \dots$ . Grimshaw & Tian (1994) discussed resonance for the fKdV equation in the presence of damping effects.

When  $k \neq \nu_c/2^n$ , for  $n \in \mathbb{N}$ , there is no resonance. In this case, for small amplitude waves,  $|\epsilon| \ll 1$ , we seek a solution as a regular expansion in the form

$$N = \epsilon N_1(x) + \epsilon^2 N_2(x) + \dots \quad (3.2)$$

Substituting into (3.1) and considering the linear problems obtained at each order of approximation, we may easily determine  $N_1(x)$ ,  $N_2(x)$ , and so on. Indeed we find

$$N_1(x) = \frac{3 \cos(kx)}{k^2 - 6\mu}, \quad (3.3)$$

which shows that small amplitude waves are in phase with the topography for frequencies

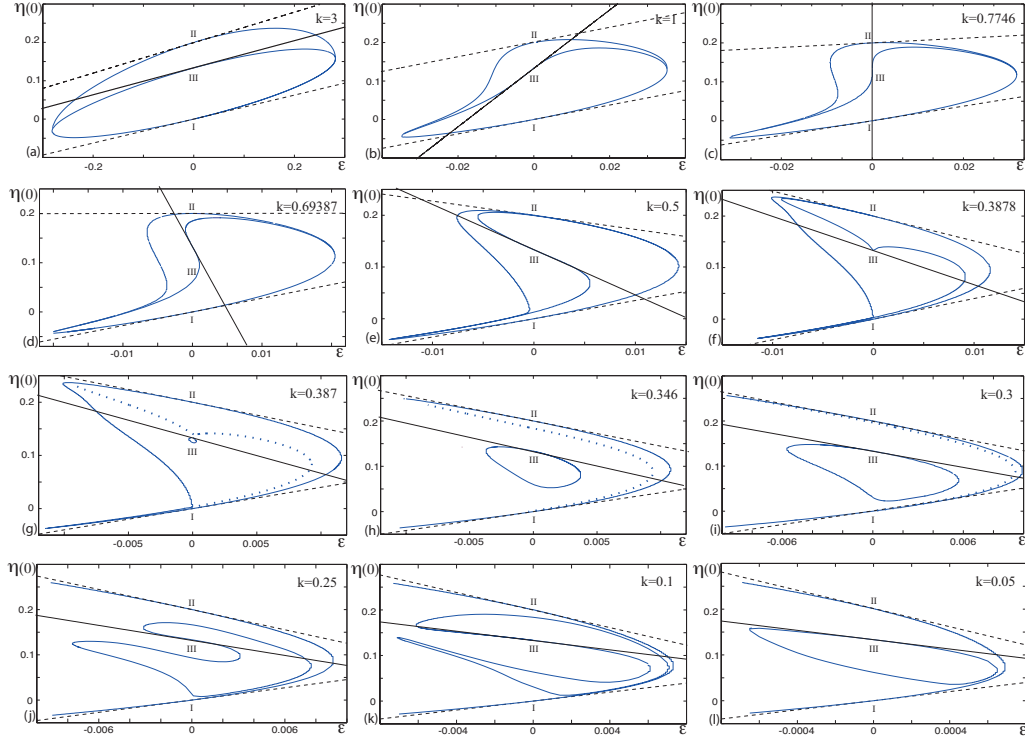


FIGURE 3. Bifurcation diagrams for the elevation of the free-surface,  $\eta(0)$ , versus amplitude of forcing,  $\epsilon$ , with  $\mu = 0.1$ . The solid curves are for the numerical solutions. The upper, middle and lower branches that emanate from the vertical axis correspond to perturbations of a uniform stream, solitary wave, and uniform cnoidal stream solutions I-III. The dotted curves in (g)–(i) are additional numerical type III solutions, as indicated by the asymptotic theory. The lower and upper broken straight lines are for the non-autonomous approximations (2.1) and (2.6), respectively. The solid straight lines are for the asymptotic theory, retaining only the first term in the regular expansion (3.2). Wavenumber forcing; (a)  $k = 3$ , (b)  $k = 1$ , (c)  $k = 0.7746$ , (d)  $k = 0.69378$ , (e)  $k = 0.5$ , (f)  $k = 0.3878$ , (g)  $k = 0.387$ , (h)  $k = 0.346$ , (i)  $k = 0.3$ . (j)  $k = 0.25$ . (k)  $k = 0.1$ . (l)  $k = 0.05$ .

above resonance,  $k > \nu_c$ , and are a half-period out of phase with the topography when  $k < \nu_c$  (in contrast with the small amplitude type I solution (2.1) which is always in phase with the topography). The dotted curve in figure 2c and the solid straight lines in the panels of figure 3 are for the asymptotic expansion (3.2), where we have retained only the first term in the expansion.

More interesting is the small amplitude response at the resonant frequencies. At primary resonance,  $k = \nu_c$ , to obtain a bounded, periodic solution, we expand in fractional powers of  $\epsilon$ , writing

$$N(x) = \epsilon^{1/3}n_1(x) + \epsilon^{2/3}n_2(x) + \epsilon n_3(x) + \dots \quad (3.4)$$

A key observation is that at second order,  $\mathcal{O}(\epsilon)$ , the first two terms in the expansion (3.4) will combine via the nonlinear term on the left hand side of (3.1) to cancel the problematic forcing term on the right hand side and thereby eliminate any secular terms. Indeed, at leading order  $\mathcal{O}(\epsilon^{1/3})$  we find  $n_1(x) = a_1 \cos kx + b_1 \sin kx$ , for constants  $a_1$

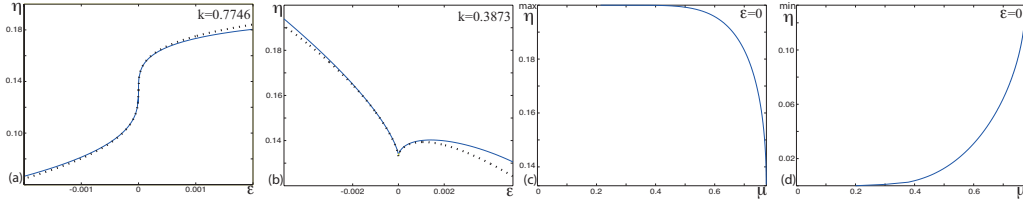


FIGURE 4. Analysis of cnoidal waves,  $\mu = 0.10$ . (a) and (b) Comparison of the type III computed solution branches (solid curves) with the asymptotic theory (dotted curves) for forcing wavenumbers  $k = 0.7746$  and  $k = 0.3873$ , respectively. In panel (a) the first two terms in the expansion (3.4) have been used; and in panel (b) the first three terms in the expansion (3.7) have been used. (c) and (d) Unforced cnoidal wave maxima/minima against wavenumber  $\nu$ ,  $\epsilon = 0$ . The wavenumber occupies  $0 \leq \nu \leq \sqrt{6\mu} = 0.7746$ . (c) Wave maximum, with  $4/3 \leq \max(\eta) \leq 0.2$ . (d) Wave minimum, with  $0 \leq \min(\eta) \leq 4/3$ .

and  $b_1$ , and at first order  $\mathcal{O}(\epsilon^{2/3})$  we obtain

$$n_2(x) = a_2 \cos kx + b_2 \sin kx + \frac{3^{5/3}}{4} \frac{(a_1^2 - b_1^2)}{k^2} \cos 2kx + \frac{3^{5/3}}{2} \frac{a_1 b_1}{k^2} \sin 2kx - \frac{3^{11/3}}{4} \frac{(a_1^2 + b_1^2)}{k^2}, \quad (3.5)$$

for constants  $a_2$  and  $b_2$ . At  $\mathcal{O}(\epsilon)$  we find that the term on the right hand side of (3.1) is eliminated if

$$a_1 = \frac{2}{3^{2/3} 5^{1/3}} k^{2/3}, \quad b_1 = 0, \quad (3.6)$$

and we obtain a periodic solution.

At the first secondary resonance, where  $k = \nu_c/2$ , we find that we must expand by writing

$$N(x) = \epsilon^{2/3} \tilde{n}_1(x) + \epsilon \tilde{n}_2(x) + \epsilon^{4/3} \tilde{n}_3(x) + \epsilon^{5/3} \tilde{n}_4(x) + \epsilon^2 \tilde{n}_5(x) + \dots \quad (3.7)$$

Working through the problems at successive orders of approximation, we find that  $\tilde{n}_1(x) = \alpha_1 \cos 2kx + \beta_1 \sin 2kx$ , for constants  $\alpha_1$  and  $\beta_1$ , and

$$\tilde{n}_2(x) = \alpha_2 \cos 2kx + \beta_2 \sin 2kx - \frac{1}{k^2} \cos kx, \quad (3.8)$$

for constants  $\alpha_2$  and  $\beta_2$ . It is now evident that the quadratic nonlinearity in (3.1) will generate, via the second term in the expansion (3.7), a resonant forcing term proportional to  $\cos \nu_c x (= \cos 2kx)$  at  $\mathcal{O}(\epsilon^2)$ . However, on noting that at next order we find

$$\tilde{n}_3(x) = \alpha_3 \cos 2kx + \beta_3 \sin 2kx + \frac{3^{1/3}}{5^{2/3} 4 k^{10/3}} (\cos 4kx - 3), \quad (3.9)$$

where  $\alpha_3$  and  $\beta_3$  are constants, it becomes clear that the problematic resonant term at  $\mathcal{O}(\epsilon^2)$  may be removed by virtue of the nonlinear interaction of the first and third terms in the expansion (3.7) and a judicious choice of the constants  $\alpha_1$  and  $\beta_1$ . Indeed, we find that the resonant term is eliminated if we choose

$$\alpha_1 = \frac{2}{3^{1/3} 5^{1/3} k^{2/3}}, \quad \beta_1 = 0, \quad (3.10)$$

to yield a periodic solution. Other secondary resonances with  $k = \nu_c/4$ , and so on, can be dealt with similarly.

In figure 4 the expansions (3.4) and (3.7) are compared against numerical results at the primary resonance and first secondary resonance for  $\mu = 0.10$ . The asymptotic solutions (3.4) and (3.7) are shown as dotted curves in figures 4a and 4b, respectively. In figure 4a

the slope of the solution curve is infinite at  $\epsilon = 0$  as is predicted by the asymptotic expansion (3.4), and in figure 4b the cusp predicted by (3.7) at  $\epsilon = 0$  is evident. The close overlap between the solid and the broken curves confirms good agreement between the asymptotic theory and the numerical computations. Furthermore, we find that the region of overlap between the solid lines and the broken lines broadens on including higher order terms in the expansions.

To interpret the numerical results, it is helpful to consider the cnoidal wave solutions which are compatible with a given forcing wavenumber  $k$ . In fact, for chosen wavenumber  $k$ , we would expect to obtain branches of periodic wave solutions which emerge continuously (as  $|\epsilon|$  is increased) from unforced cnoidal wave solutions at  $\epsilon = 0$  if the cnoidal wavenumber,  $m$ , is a rational multiple of  $k$ , that is if  $m = rk$  for  $r \in \mathbb{Q}$ . If we restrict our numerical computations to a truncated domain containing just one wavelength, then we instead require either  $r \in \mathbb{N}$  giving superharmonic cnoidal waves, or  $1/r \in \mathbb{N}$  giving subharmonic cnoidal waves. To this end, it will be useful to consider the possible unforced cnoidal wave frequencies for given values of  $\mu$  and  $k$ . We restrict attention to superharmonic cnoidal waves, that is waves with wavelength a fraction of the forcing period, and assume that  $r \in \mathbb{N}$ . To inform the discussion in the next section, we present in figures 4c and 4d, the maxima and minima of the family of cnoidal waves obtained as periodic solutions to the fully nonlinear problem (3.1) for the case  $\mu = 0.1$ . The curves are plotted against the wavenumber  $\nu$ . In the limit of small amplitude cnoidal waves, corresponding to circuits tight around the point III in figure 1b,  $\max(\eta)$  and  $\min(\eta)$  both approach the value  $4\mu/3 = 1.333$ , and the wavenumber  $\nu$  approaches the critical value  $\nu_c = 0.7746$ .

#### 4. Discussion

Here we further discuss the morphology in the solution structure of figure 3, in particular the dependence on the wavenumber  $k$ . The solid curves are for the numerical solutions with  $\mu = 0.10$ . The lower and upper broken straight lines are for the non-autonomous approximations (2.1) and (2.6), respectively. The solid straight lines are for the asymptotic theory, retaining only the first term in the regular expansion (3.2). We begin by discussing the branches which emerge from the three unforced solutions I–III in figure 3a, where  $k = 3.0$ . For either  $\epsilon < 0$  or  $\epsilon > 0$ , the three branches I–III intersect at  $\epsilon \approx -0.28$  and  $\epsilon \approx 0.28$ , respectively. The solutions on branch I and III with a wave crest at  $x = 0$  for  $0 < \epsilon \leq 0.28$  (e.g. figures 2a and 2c) are the same as their corresponding solutions found on branches I and III with a wave trough at  $x = 0$  for  $-0.28 \leq \epsilon < 0$ . For this value of  $k = 3.0$ , the crests and troughs of the free-surface elevation and forcing are in-phase for both solutions I and III. Moreover, the flow type I solutions remain in-phase with the topography for all values of  $k$ .

We find two qualitatively different solutions on the branches of flow type II that emanate from  $\eta(0) = 2\mu$  in figure 3a. For amplitude of forcing  $\epsilon > -0.03$  solutions are characterised by a maximum elevation at  $x = 0$  that coincides with a wave crest on the topography, close to the maximum elevation of the unforced solitary wave (figure 2b). When  $\epsilon < -0.03$  the solutions are characterised by a trough at  $x = 0$  (figure 2d). The two qualitatively different sub-types of solution II both have an overall shape that is characteristic of the unforced solitary wave with perturbations that are in-phase with the channel bottom topography. A similar structure of solutions is found for higher values of the forcing wavenumber (not shown) with a corresponding increasing number of fluctuations to the overall solitary wave shape. In contrast, the number of fluctuations to the overall solitary wave shape of the type II solutions decreases as  $k$  decreases.

At the resonant forcing wavenumber  $k = \nu_c \approx 0.7746$ , we expect a change in the



solution structure with regard to the type III cnoidal solutions, as discussed in section 3. The solution space at this wavenumber is shown in figure 3c. Perhaps the most notable feature is that for some values of  $\epsilon < 0$  there are three sub-types of solution II (figures 5a–5c), but only one sub-type of type II solutions when  $\epsilon > 0$ . The vertical branch of type III solutions at  $\eta = 0$  was discussed in section 3 and successfully compared with the predictions of asymptotic theory.

When  $k < \nu_c$  there exists non-flat cnoidal wave solutions at  $\epsilon = 0$ . Figure 3d shows the solution space at  $k = 0.69378$ , just below  $\nu_c$ . Notice that these type III solution branches connect with the vertical axis in figure 3d at three values of  $\eta(0)$ , corresponding to a solution with a flat free surface ( $\eta(0) = 0.33$ ), a solution with its maximum  $\eta = 0.185$  above the topography maximum at  $x = 0$ , and a third solution with its minimum  $\eta = 0.061$  above the topography maximum at  $x = 0$  (these maximum/minimum values can be read off the curves in figures 4c and 4d). Sample type III periodic wave profiles are shown in figures 5d–5f for small positive  $\epsilon$ . Two of these have a free-surface out of phase with the topography as  $\epsilon \rightarrow 0$ , with a trough immediately above a topography crest (figures 5e and 5f), while the other is in phase with a crest above a topography crest.

The solution space shown at  $k = 0.5$  in figure 3e is qualitatively similar to that shown in figure 3d. A further structural change occurs at the first secondary resonance  $k = \nu_c/2 = 0.3872$  where a cusp is expected in the type III solution branch at  $\epsilon = 0$  (see figure 4). Figure 3f shows the solution space at  $k = 0.3878$ , just above the secondary resonance frequency. The near formation of the cusp is clearly visible. Note that there are still three qualitatively different type III solutions, but, as can be seen from figures 4c and 4d two of them have  $\eta(0)$  very close to 0.2 and 0 respectively, and so their solution branches almost coincide with those found for the flow types I and II (figure 3f). The wave profiles on the branches which almost overlie these type III branches around  $\epsilon = 0$  now have a smaller wave crest that is in-phase with topography (figure 5h), with the larger wave crests being out of phase with the forcing.

When  $k < \nu_c/2$ , according to the discussion in section 3, superharmonic unforced cnoidal wave solutions are possible at  $\epsilon = 0$ , and this suggests the appearance of further branches of solution. Indeed, just after the type III solution cusp forms at  $k = \nu_c$ , a closed loop of type III solutions is created immediately below  $\eta = 0.133$ . This loop grows in size as  $k$  is lowered, as can be seen in figures 3g–3i. Figures 5j and 5k shows typical wave profiles on the closed-loop solution branch for figure 3i. In all there are five type III solution branches emerging from  $\epsilon = 0$  in figures 3g–3i. Three of these branches are as shown: at  $\epsilon = 0$  they correspond to a flat free surface, with  $\epsilon = 0.133$ , and two superharmonic cnoidal waves of frequency  $\nu = 2k$  which are in phase with, and one half-period out of phase with, the topography respectively. The maxima and minima on these waves can be read from the curves in figures 4c and 4d. These imply the presence of two further solution branches (not shown) emerging from unforced solutions at  $\epsilon = 0$  with values of  $\eta(0)$  which are very close to 0.2 and 0 respectively. Note that there is now only one sub-type of solution for flow type II with  $\epsilon < 0$  (figure 5l).

When  $k < \nu_c/3 = 0.2582$ , further superharmonic unforced cnoidal waves come into play and herald the appearance of more solution branches in the  $(\epsilon, \eta(0))$  plane. For example, at  $k = 0.25$  shown in figure 3j the closed loop has deformed to admit four unforced cnoidal wave solutions at  $\epsilon = 0$ . In total there are seven unforced cnoidal wave solutions at this wavenumber, with non-flat solutions having frequencies  $k$ ,  $2k$  and  $3k$  (in each case two waves are possible, either in or out of phase with the topography). According to figure 4c and 4d some of the corresponding solution branches emerge from values of  $\eta(0)$  very close to 0.2 and 0, and we have not attempted to delineate them in figure 3j.

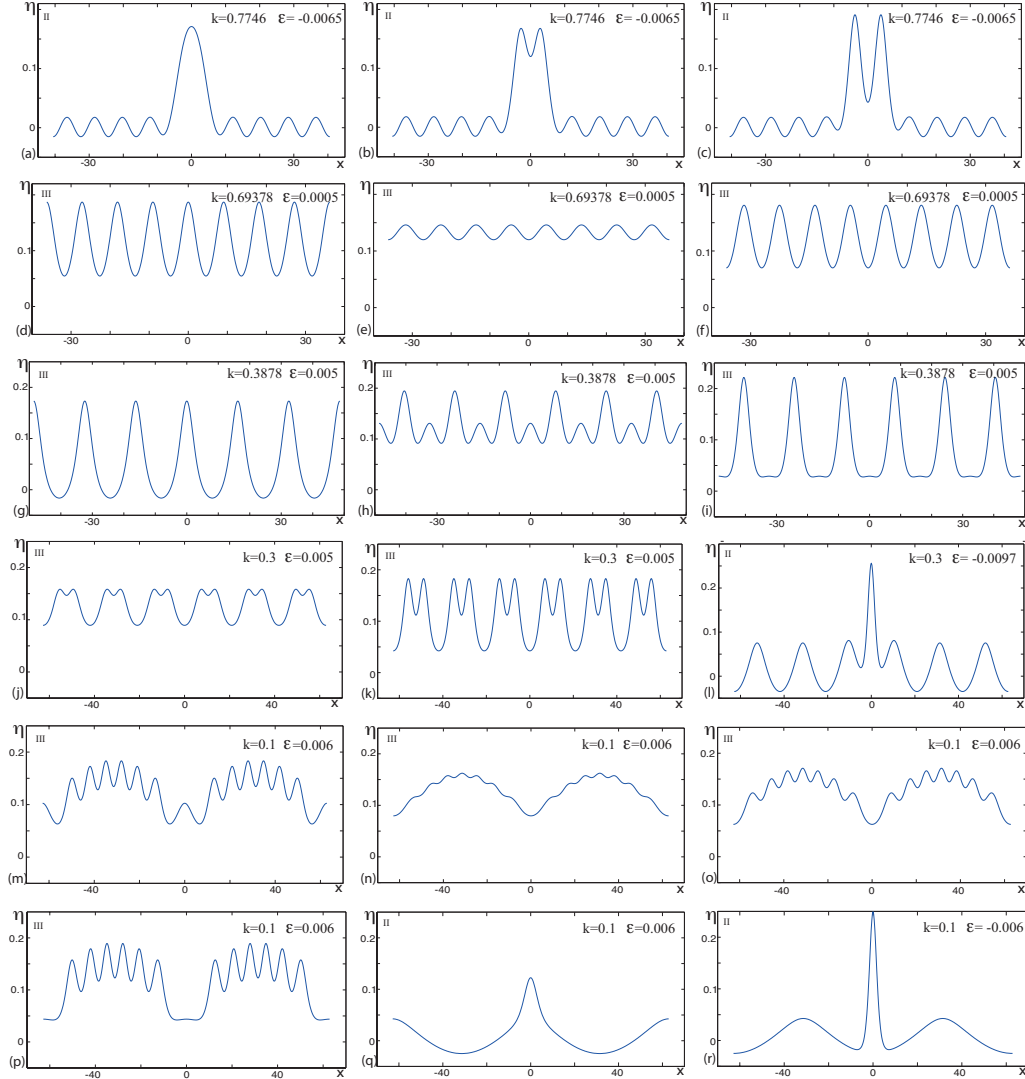


FIGURE 5. Free-surface profiles for  $\mu = 0.10$ . (a)–(c)  $k = 0.7746$ ,  $\epsilon = -0.0065$ ; (a)  $\eta(0) = 0.171$ , (b)  $\eta(0) = 0.120$ , (c)  $\eta(0) = 0.043$ . (d)–(f)  $k = 0.69378$ ,  $\epsilon = 0.0005$ ; (d)  $\eta(0) = 0.187$ , (e)  $\eta(0) = 0.120$ , (f)  $\eta(0) = 0.070$ . (g)–(i)  $k = 0.3878$ ,  $\epsilon = 0.005$ ; (g)  $\eta(0) = 0.173$ , (h)  $\eta(0) = 0.131$ , (i)  $\eta(0) = 0.029$ . (j)–(l)  $k = 0.3$ ; (j)  $\epsilon = 0.005$ ,  $\eta(0) = 0.089$ , (k)  $\epsilon = 0.005$ ,  $\eta(0) = 0.057$ , (l)  $\epsilon = -0.0097$ ,  $\eta(0) = 0.256$ . (m)–(q)  $k = 0.1$ ,  $\epsilon = 0.006$ ; (m)  $\eta(0) = 0.103$ , (n)  $\eta(0) = 0.0796$ , (o)  $\eta(0) = 0.0626$ , (p)  $\eta(0) = 0.044$ , (q)  $\eta(0) = 0.1225$ . (r)  $k = 0.1$ ,  $\epsilon = -0.006$ ,  $\eta(0) = 0.2495$ .

Reducing  $k$  still further presents the possibility of more superharmonic cnoidal waves and further secondary resonances, increasing the complexity of the solution space. Figure 3k shows the solution space for  $k = 0.1$ , which lies below the next secondary resonance at  $k = \nu_c/4 = 0.1936$ . Note that in this figure we only show the closed loop solution branch, and ignore the numerous other branches which emerge from  $\epsilon = 0$ . Figures 5m–5p show type III typical wave profiles on the closed loop in figure 3k.

Although we have focused our attention on branches that emanate from the unforced solutions I–III, the non-autonomous theory indicates that there are infinitely many to be found. The numerical solutions in figures 2e and 2f are a case in point; they are

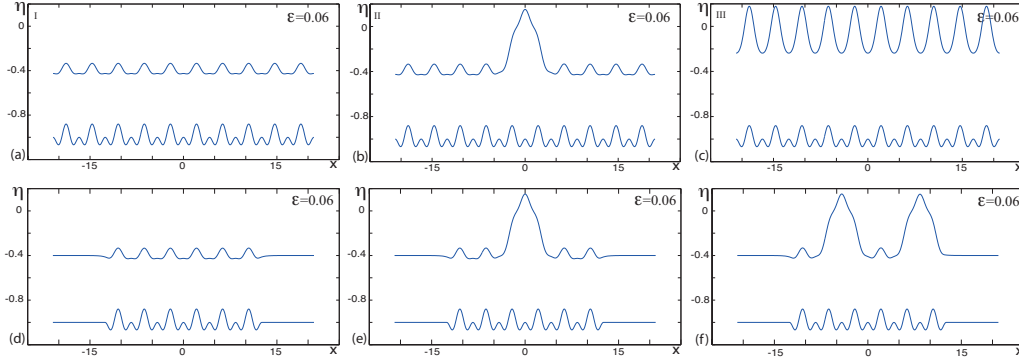


FIGURE 6. Free-surface profiles with  $\mu = -0.3$ ,  $k = 3.0$ ,  $\epsilon = 0.06$ . (a)–(c) The topography is given by equation (4.1). (a) Perturbation of a uniform stream solution I. (b) Perturbation of a solitary wave solution II. (c) Perturbation of a uniform cnoidal stream solution III. (d)–(f) Additional solutions for compact topography given by equation (4.2),  $m = 3$ .

approximately the superposition of several of the type-II waves that we have analytically described, and were found by using such a superposition as an initial guess in the Newton iterative method.

The bifurcation structure of the cnoidal waves has particular relevance when considering  $\mu < 0$ . If so, the phase diagram for the unforced problem is the same as that shown in figure 1b, but with a translation in  $\eta$  of  $4\mu/3$  to the left: the saddle is now at  $(4\mu/3, 0)$ , this has an attached homoclinic orbit with maximum  $\eta = -2\mu/3$ , and the centre—the uniform cnoidal stream—is at  $(0, 0)$ . Since this satisfies the far-field conditions  $\eta_{xx} \rightarrow 0$ ,  $\eta_x \rightarrow 0$ ,  $\eta \rightarrow 0$  as  $x \rightarrow \pm\infty$ , the cnoidal stream (solution type III) is physically meaningful. On the other hand, the invariance as expressed in (1.4) shows the equivalence of this physical solution for  $\mu < 0$ , and the uniform cnoidal stream for  $\mu > 0$ . Thus our analysis of the cnoidal bifurcation structure for  $\mu > 0$  is directly applicable to the bifurcations of the physically-relevant  $\mu < 0$  cnoidal waves.

Accordingly, we address  $\mu < 0$  in our next example group of examples. First, we choose

$$\sigma(x) = \epsilon \left( \cos kx - \cos \left( \frac{kx}{2} \right) \right), \quad (4.1)$$

for which numerical solutions are shown in figures 6(a)–(c). Comparison of the plots shown in figures 6(a)–(c) with those in figures 2(a)–(c) indicate that our method of analysis of the solution structure (e.g. figure 3) can be applied to other periodic topographies in either a  $\mu > 0$  or  $\mu < 0$  flow regime.

The last example of forcing we consider has compact support, given by

$$\sigma(x) = \begin{cases} \epsilon \left( \cos kx - \cos \left( \frac{kx}{2} \right) \right) & \text{if } |x| \leq \frac{4\pi m}{k} \\ 0 & \text{if else} \end{cases}, \quad (4.2)$$

and the results presented in figures 6(d)–(f) can be viewed as type I, type II, and combined-type-II, solutions. In general, there are only finitely many near-solitary waves for compactly supported topography. Further examination of the solution structure in flows with  $\mu \leq 0$  for general forcing is left to future research, and we note that Binder et al. (2014) considered the case of compact periodic forcing when  $\mu = 0$ .

## 5. Concluding remarks

We have studied solutions to the forced Korteweg-de Vries equation under periodic forcing as a model for the flow of water over a spatially periodic bed. We have computed new near-solitary wave solutions, which have periodic tails in the far field. Solutions with a peak of the solitary wave over each crest in the bed, and solutions with a peak of the solitary wave over each trough in the bed, are both possible. We have also found many bound-state solutions in the same flow which are approximately the superposition of several of these solitary-type waves. It is worth emphasising that in the unforced case (flat bed) the translational invariance of the KdV equation means that the classical  $\text{sech}^2$  solution, given by (1.3), may be translated by an arbitrary amount to construct infinitely many acceptable solutions; however it is not permissible to superpose two such solutions to form a multi-humped solution.

It is interesting to draw a connection between the new solutions discussed in the present work and known behaviour in the problem of resonant sloshing in a horizontally oscillating water tank (e.g. Ockendon *et al.* 1986; Amundsen *et al.* 2007). In the latter problem the fKdV equation arises in the limit of small amplitude oscillations and shallow water. When the driving frequency is close to resonance, Ockendon *et al.* (1986) used an asymptotic analysis to obtain periodic solutions with very rapid and short-lived spiked bursts occurring at regular intervals in the time signal. Local solutions are constructed inside each of the rapid burst regions; these solutions have a solitary-type character which are not dissimilar to those we have presented in figure 2 (see their figure 4, for example). We emphasise, however, that these local solutions form part of an overall periodic solution. Our solutions are of genuine solitary-type character, are non-periodic, and have a clear physical interpretation in the context of flow over a corrugated bed.

We have left open here the issue of whether the solutions we have computed are stable or unstable, and work on this question is currently underway. The physical relevance of the new solitary-type solutions to fKdV which we have constructed must also be tested by seeking solutions of this type to the fully nonlinear water wave problem. This will also form the subject of a future investigation.

## Acknowledgments

SB was supported by the Australian Research Council grant FT130100484.

## REFERENCES

- AKYLAS, T. R. 1984 On the excitation of long nonlinear water waves by a moving pressure distribution. *J. Fluid Mech.* **141**, 455–466.
- AMUNDSEN, D. E., COX, E. A. & MORTELL, M. P. 2007 Asymptotic analysis of steady solutions of the KdVB equation with application to resonant sloshing. *Z. angew. Math. Phys.*, **58**, 1008–1034.
- BALASURIYA, S. 2005 Optimal perturbation for enhanced chaotic transport. *Phys. D* **202**, 155.
- BALASURIYA, S. & FINN, M. D. 2012 Energy-constrained transport maximization across a fluid interface. *Phys. Rev. Lett.* **108**, 244503.
- BALASURIYA, S. & PADBERG-GEHLE, K. 2013 Controlling the unsteady analogue of saddle stagnation points. *SIAM J. Appl. Math.* **73**, 1038.
- BALASURIYA, S. & PADBERG-GEHLE, K. 2014 Accurate control of hyperbolic trajectories in any dimension. *Phys. Rev. E* **90**, 032903.
- BALASURIYA, S. & BINDER, B. J. 2014 Nonautonomous analysis of steady Korteweg-de Vries waves under nonlocalised forcing. *Phys. D* **285**, 28–41.
- BILLINGHAM, J. & KING, A. C. 2000 *Waves Motion*. Cambridge University Press.

- BINDER, B. J., DIAS, F. & VANDEN-BROECK, J.-M. 2005 Forced solitary waves and fronts past submerged obstacles. *Chaos* **15**, 037106.
- BINDER, B. J., BLYTH M. G. & MCCUE, S. W. 2013 Free-surface flow past arbitrary topography and an inverse approach for wave-free solutions. *IMA J. Appl. Math.* **78**, 685 .
- BINDER, B. J., BLYTH, M. G. & BALASURIYA, S. 2014 Non-uniqueness of steady free-surface flow at critical Froude number *EPL* **105**, 44003.
- COLE, S. L. 1985. Transient waves produced by flow past a bump. *Wave Motion* **7**, 579–587.
- COX, E. A. & MORTELL, M. P. 1986 The evolution of resonant water-wave oscillations, *J. Fluid Mech.*, **162**, 99–116.
- DAVIES, A. G. & HEATHERSHAW, A. D. 1984 Surface-wave propagation over sinusoidally varying topography. *J. Fluid Mech.* **144**, 419–443.
- DIAS, F. & VANDEN-BROECK, J.-M. 2002 Generalised critical free-surface flows. *J. Eng. Math.* **42**, 291.
- GRIMSHAW, R. H. J., & SMYTH, N. 1986 Resonant flow of a stratified fluid over topography *J. Fluid Mech.* **169**, 429–464.
- GRIMSHAW, R. & TIAN, X. 1994 Periodic and chaotic behaviour in a reduction of the perturbed Korteweg-de Vries equation. *Proc. R. Soc. Lond. A* **445**, 1–21.
- GUCKENHEIMER, J. & HOLMES, P. J. 1983 *Nonlinear Oscillations, Dynamical Systems, and Bifurcation of Vector Fields*, Springer.
- LAMB, H. 1879 *Hydrodynamics*. Cambridge University Press.
- LIGHTHILL, M. J. 1978 *Waves In Fluids*. Cambridge University Press.
- OCKENDON, J. R. & OCKENDON, H. 1973 Resonant surface waves, *J. Fluid Mech.*, **59**, 397–413.
- OCKENDON, H., OCKENDON, J. R. & JOHNSON, A. D. 1986 Resonant sloshing in shallow water, *J. Fluid Mech.*, **167**, 465–479.
- REYNOLDS, A. J. 1965 Waves on the erodible bed of an open channel, *J. Fluid Mech.* **22**, 113–133.
- ROM-KEDAR, V., LEONARD, A. & WIGGINS, S. 1990 An analytical study of transport, mixing and chaos in an unsteady vortical flow. *J. Fluid Mech.* **214** 347.
- SHEN, S. S-P. 1993 *A Course on Nonlinear Waves*. *Kluwer Academic Publishers*.
- WU, T. 1987 Generation of upstream advancing solitons by moving disturbances. *J. Fluid Mech.* **184**, 75–99.